

Influence of elastic and inelastic scattering on energy spectra of electrons emitted from solids

Sven Tougaard and Peter Sigmund

Fysisk Institut, Odense Universitet, DK-5230 Odense M, Denmark

(Received 1 September 1981)

We have investigated theoretically the spectrum of electrons emitted from a solid in the case of a primary excitation function corresponding to a narrow line as in Auger and photoelectron spectroscopy. We concentrate on the influence of elastic and inelastic electron scattering on the shape and intensity of the spectrum in the vicinity of the primary peak. A near-peak as well as an off-peak region is identified; the critical energy loss separating the two regions is shown to depend on the relative significance of angular deflection and inelastic scattering. A rigorous formula has been derived that allows the extraction of the primary spectrum from a measured electron current if the normalized energy-loss function is available. The physical significance of the escape depth extracted from experiments with overlayers is analyzed. We find that it is not justified in general to identify the escape depth measured by means of overlayers with the inelastic mean free path.

I. INTRODUCTION

Auger and x-ray photoelectron spectroscopy (AES and XPS) are now widely used techniques for the investigation of solid surfaces. They give information on elemental composition as well as electronic states in the surface region of materials.¹ Photoelectrons are usually recorded as direct energy spectra $N(E)dE$, with E being the electron energy, and peak areas are used for the purpose of quantitative analysis. Auger electrons are most often recorded as differentiated spectra, at least for the purpose of *qualitative* analysis, since this procedure most readily removes the background signal from (usually rather weak) Auger lines.

Due to chemically induced changes in line shape,² which can occur, the intensity in the derivative spectrum³ (measured by, e.g., the zero-to-peak or peak-to-peak amplitude) is not in general a good quantity for use in *quantitative* analysis. Therefore, it has been argued that peak areas as determined from the direct energy spectrum $N(E)$ are to be preferred in quantitative Auger analysis.⁴

The line shape of Auger and photoelectron spectra contains important information on the electronic structure of solids. Thus, the detailed energy distribution of emitted electrons gives information on basic electronic and chemical properties of materials.¹

Figure 1 shows a typical photoelectron spectrum from a metal (gold). The peaks in the spectrum correspond to kinetic energies of photon-excited electronic states in the metal. Measured line profiles will be influenced by instrumental resolution, photon energy width, and core level widths. The instrumental broadening can in principle be minimized by improved energy resolution.

Electronic energy levels in solids differ in general

from those of the corresponding free atoms. In addition, the energy distribution of excited electrons is determined by lifetime broadening and the electrostatic screening by conduction electrons of the core hole created in the excitation process.⁵ This latter effect results in a weak tail on the low-energy side of the peak.⁶ This asymmetry of XPS peaks which extends a couple of electron volts below the peak energy has been observed experimentally for a number of materials and is well understood for simple metals.⁷

Auger peaks are usually broader than photoelectron lines. Auger peaks of interest to surface analysis usually involve electrons from valence and have a width of typically several electron volts. The observed shape of an Auger line for a CVV (core-valence-valence) transition is essentially determined by a convolution of two electronic densities of states, with a resulting typical width much larger than that observed for XPS peaks.

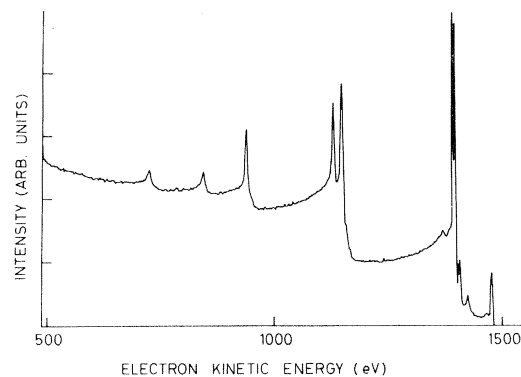


FIG. 1. Photoelectron spectrum of polycrystalline gold. Courtesy of I. Alstrup, Haldor Topsøe Laboratory, Copenhagen.

From Fig. 1 it is evident that every peak is accompanied by an increased background intensity at the low-energy side. This tail (hereafter defined as the background signal associated with the peak) corresponds to electrons that have suffered inelastic collisions in the material. This background signal can be followed over an energy range of several hundred electron volts (Fig. 1). Figure 2 shows schematically a measured spectrum in the region around a single peak, any possible structure in the background signal being neglected.

The background signal constitutes a major problem in the application of electron spectroscopy to surface analysis. Correction must be made for this effect before a determination of the true peak area or line shape is possible. Therefore, a theoretical description is needed. Several authors have discussed the problem,⁸⁻¹⁴ yet the procedures proposed are essentially empirical.

In XPS, the method of Shirley¹⁰ is frequently used. Here, the background intensity within a peak is assumed proportional to the integrated intensity at higher energy with the condition that the background matches the measured spectrum outside the region of the peak (Fig. 2). Sickafus¹¹ proposed a procedure for background subtraction in AES involving straight lines in a double logarithmic plot. For background subtraction in ultraviolet photoemission spectroscopy, Berglund and Spicer¹² considered a simple model involving singly scattered electrons. Madden and Houston¹³ have applied deconvoluting methods in which the spectrum of inelastically backscattered electrons resulting from bombarding the surface with monoenergetic electrons is an essential factor. This

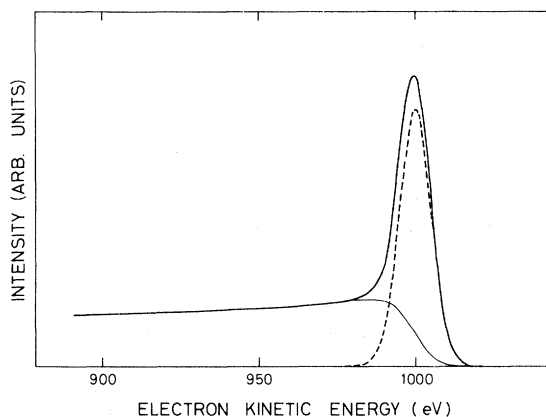


FIG. 2. Schematic representation of measured electron spectrum for Gaussian line shape of primary excitation profile. Superimposed on the primary spectrum is a continuous background due to inelastically scattered electrons. Note the increase of the background signal near the primary energy. Also shown is a background spectrum calculated on the basis of a widely used empirical method (Ref. 10). See text.

spectrum, however, refers to a somewhat different situation from that of XPS and AES where electrons emitted are located inside the solid.¹⁵

In the present work we consider distortions in electron spectra caused by inelastic scattering events during electron transport from the point of excitation to the surface. The theoretical scheme is based on standard theory of particle transport in random media. The basic tools have been summed up recently.¹⁶ As the experimental resolution in XPS and AES is typically of the order 1 eV we shall in this work define scattering on phonons as elastic scattering.

It is obvious that the background signal must depend on the depth distribution of electron emitters in the material. Therefore, the shape of the background signal must carry information on the depth distribution of a given element in the surface region of the material. This point will be briefly touched upon in the present paper and will be treated in more detail in subsequent work.

II. GENERAL DESCRIPTION

Consider the physical situation sketched in Fig. 3. Electrons are excited (by Auger transitions or photon absorption) in a semi-infinite solid with a plane surface. The problem consists in finding the energy distribution of those electrons that escape through the surface and enter the electron energy analyzer.

An individual electron with initial energy E_0 created at depth x below the surface (Fig. 3) will suffer inelastic as well as elastic collisions during transport in the solid. It is the inelastic scattering events that are responsible for the experimental observation (see Figs. 1 and 2) that an emitted electron may have a kinetic energy E below E_0 . Elastic scattering will also be of importance. Indeed, angular deflection will

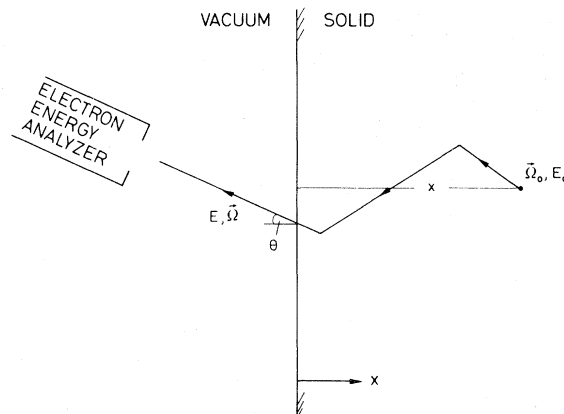


FIG. 3. Emission of an electron excited at depth x . Geometry and notation.

cause deviations from straight-path motion in the solid and thus increase the total path length traveled by an electron before it reaches the surface. The number of inelastic events increases with the total path length traveled in the solid.

Let $F(E_0, \bar{\Omega}_0, x)$ be the primary excitation spectrum, i.e., $F(E_0, \bar{\Omega}_0, x) dE_0 d^2 \bar{\Omega}_0 dx$ is the mean number of electrons excited at depth (x, dx) in an energy interval (E_0, dE_0) into the solid angle $(\bar{\Omega}_0, d^2 \bar{\Omega}_0)$ per bombarding particle (photon, electron, ion, etc.). Moreover, let $P(E_0, \bar{\Omega}_0, x; E, \bar{\Omega}) dE d^2 \bar{\Omega}$ be the probability for an electron of initial energy E_0 and direction $\bar{\Omega}_0$, generated at depth x , to arrive at the target surface with an energy (E, dE) and direction $(\bar{\Omega}, d^2 \bar{\Omega})$. Then, the emitted electron flux $J(E, \bar{\Omega}) dE d^2 \bar{\Omega}$ is given by

$$J(E, \bar{\Omega}) = \int dE_0 \int d^2 \bar{\Omega}_0 \int dx F(E_0, \bar{\Omega}_0, x) \times P(E_0, \bar{\Omega}_0, x; E, \bar{\Omega}) , \quad (1)$$

except for an energy shift and an angular deflection at the surface caused by the work function of the material; this effect is easily incorporated when necessary, but negligible for $E \geq 100$ eV.

The primary spectrum, $F(E_0, \bar{\Omega}_0, x)$, contains the elementary excitation spectrum which depends on the type and energy of the primary irradiating particle. The depth dependence is determined by the attenuation of the primary beam as well as the composition of the medium. We shall mainly deal with isotropic excitation, i.e.,

$$F(E_0, \bar{\Omega}_0, x) \equiv F(E_0, x) ; \quad (2)$$

this implies that the propagator function P can be determined for an isotropic source, hence

$$P = P(E_0, x; E, \bar{\Omega}) . \quad (2a)$$

The effect of elastic and inelastic scattering is contained in the propagator function $P(E_0, x; E, \bar{\Omega})$. The determination of this type of function belongs to the subject of electron transport theory.

Consider first the case of slowing down *without* angular deflection. Then, we may write

$$J(E, \bar{\Omega}) = \int dE_0 \int dx F(E_0, x) G(E_0, R; E) , \quad (3)$$

with

$$R = x / \cos \theta , \quad (4)$$

where $G(E_0, R; E) dE$ is the probability for the electron to have an energy (E, dE) after having travelled a path length R , and θ is the angle between $\bar{\Omega}$ and the outward surface normal (Fig. 3). Let us now consider the case of non-negligible angular deflection. Noting that in the vicinity of the peak the relative energy loss and hence the angular deflection in an in-

elastic scattering event is small, we find effects of elastic and inelastic scattering to be separable, i.e.,

$$P(E_0, \bar{\Omega}_0, x; E, \bar{\Omega}) = \int dR Q(E_0, \bar{\Omega}_0, x; R, \bar{\Omega}) \times G(E_0, R; E) , \quad (5)$$

where $Q(E_0, \bar{\Omega}_0, x; R, \bar{\Omega}) dR d^2 \bar{\Omega}$ is the probability for the electron to arrive at the surface moving in the direction $(\bar{\Omega}, d^2 \bar{\Omega})$ after having travelled a path length (R, dR) .

We shall first consider the case of negligible angular deflection, Eqs. (3) and (4), and treat Eq. (5) subsequently. In either case, we shall restrict our attention to the case of small relative energy loss, $|E_0 - E| \ll E_0$.

III. ELECTRON ENERGY LOSS

Let $K(E, T) dT \delta R$ be the probability for an electron with energy E to undergo an inelastic scattering event with energy loss (T, dT) while traveling a path length element δR , i.e., $K(E, T)$ is the inverse differential mean free path for inelastic scattering. $K(E, T)$ depends in general strongly on T but only weakly on E . Hence, for path lengths sufficiently small so that the mean relative energy loss is small, one may ignore the dependence of K on E as a first approximation.

In that latter case, the multiple scattering problem has a rigorous solution. The energy distribution $G(E_0, R; E)$ is given by Landau's formula¹⁷

$$G(E_0, R; E) = \frac{1}{2\pi} \int_{-\infty}^{\infty} ds \exp[is\epsilon - R\Sigma(s)] , \quad (6)$$

where

$$\epsilon = E_0 - E \quad (7)$$

and

$$\Sigma(s) = \int_0^{\infty} dT K(T) (1 - e^{-isT}) . \quad (8)$$

For moderate energy loss, the validity of Eq. (6) may be extended by means of the replacement

$$R\Sigma(s) \rightarrow \int_0^R dR' \Sigma(E(R'), s) , \quad (9)$$

where $E(R')$ is the *mean electron energy* after path length R' .

The function $K(E, T)$ shows in general some structure, e.g., due to plasmon excitations at $T \approx \hbar\omega_p$, ω_p being the plasma frequency, as well as a broad continuum up to the maximum attainable energy transfer, which is usually defined as $T_{\max} = E/2$ in view of the indistinguishability of individual electrons. Although low-energy transfers are preferred, K approaches zero for $T \rightarrow 0$. In metals, this approach must be linear at sufficiently low T . This gen-

eral property has been demonstrated for the free electron gas.¹⁸ In insulators, K will be zero for values of T below the lowest level of excitation.

A. Small energy loss

For small energy loss, $\epsilon \lesssim 20$ eV, only a very small number of scattering events can contribute to the spectrum, and the discrete features must dominate. Hence, we may expand the exponential in (6) according to

$$e^{-R\Sigma(s)} = e^{-R/\lambda} \left[1 + R \int dT K(T) e^{-isT} + \frac{1}{2} R^2 \int dT K(T) \int dT' K(T') \exp[-is(T+T')] + \dots \right], \quad (10)$$

with

$$\frac{1}{\lambda} = \int_0^\infty dT K(T). \quad (11)$$

From (10), we find the spectrum

$$G(E_0, R; E) = e^{-R/\lambda} \left[\delta(\epsilon) + RK(\epsilon) + \frac{1}{2} R^2 \int_0^\infty dT K(T) K(\epsilon - T) \dots \right]. \quad (12)$$

The first term in the large parentheses of Eq. (12) represents the zero-loss portion of the spectrum, while the second term corresponds to a single event, the third a double event, etc.

As an example, consider a system with plasmon loss only, according to

$$K(T) \simeq \frac{1}{\lambda_P} \delta(T - \hbar\omega_P), \quad (12')$$

where λ_P is the mean free path for plasmon generation. Then, (12) yields

$$G(E_0, R; E) = e^{-R/\lambda_P} \left[\delta(\epsilon) + \frac{R}{\lambda_P} \delta(\epsilon - \hbar\omega_P) + \frac{1}{2} \left(\frac{R}{\lambda_P} \right)^2 \delta(\epsilon - 2\hbar\omega_P) + \dots \right], \quad (13)$$

where the coefficients correspond to the familiar Poisson distribution.

Next, consider the linear portion for small energy losses,

$$K(T) \simeq AT, \quad T < T_0, \quad (14)$$

where A is a constant and T_0 some limiting energy below any discrete energy-loss peak. Here, we find

$$G(E_0, R; E) = e^{-R/\lambda} \left[\delta(\epsilon) + RA\epsilon + \frac{1}{12} A^2 R^2 \epsilon^3 \dots \right], \quad (15)$$

where λ is still defined according to (11).

B. Larger energy loss

For ϵ exceeding those energies where the discrete features dominate the spectrum, a continuum description of energy loss is appropriate.¹⁹ Expand (8) in powers of s ,

$$\Sigma(s) = isS + \frac{1}{2} s^2 W \dots, \quad (16)$$

with

$$S = \int KT dT; \quad W = \int KT^2 dT. \quad (17)$$

Then, Eq. (6) reads¹⁹

$$G(E_0, R; E) = \frac{1}{(2\pi WR)^{1/2}} \exp\left[-\frac{(\epsilon - RS)^2}{2RW}\right], \quad (18)$$

i.e., one expects a Gaussian energy spectrum centering around the mean energy loss RS with a variance

RW . If applying the substitution (9), we find the mean energy loss

$$\langle \epsilon \rangle \simeq \int_0^R dR' S(E(R')) \quad (19a)$$

and the variance

$$\langle (\epsilon - \langle \epsilon \rangle)^2 \rangle \simeq \int_0^R dR' W(E(R')). \quad (19b)$$

$S = S(E)$ and $W = W(E)$ are the well-known expressions for stopping power and straggling parameter.¹⁹

As an even simpler approximation, one may be tempted to approximate (18) by a δ function

$$G(E_0, R; E) \simeq \delta(\epsilon - RS); \quad (18')$$

the relative accuracy of this approximation increases with increasing R .

C. An example

As an example, consider the energy-loss function

$$K(T) = ATe^{-\beta T}; \quad 0 \leq T < \infty, \quad (20)$$

which yields

$$\lambda = \beta^2/A, \quad S = 2/\beta\lambda, \quad W = \frac{3}{2}\lambda S^2, \quad (21)$$

and

$$\Sigma(s) = A \left[\frac{1}{\beta^2} - \frac{1}{(\beta + is)^2} \right]. \quad (22)$$

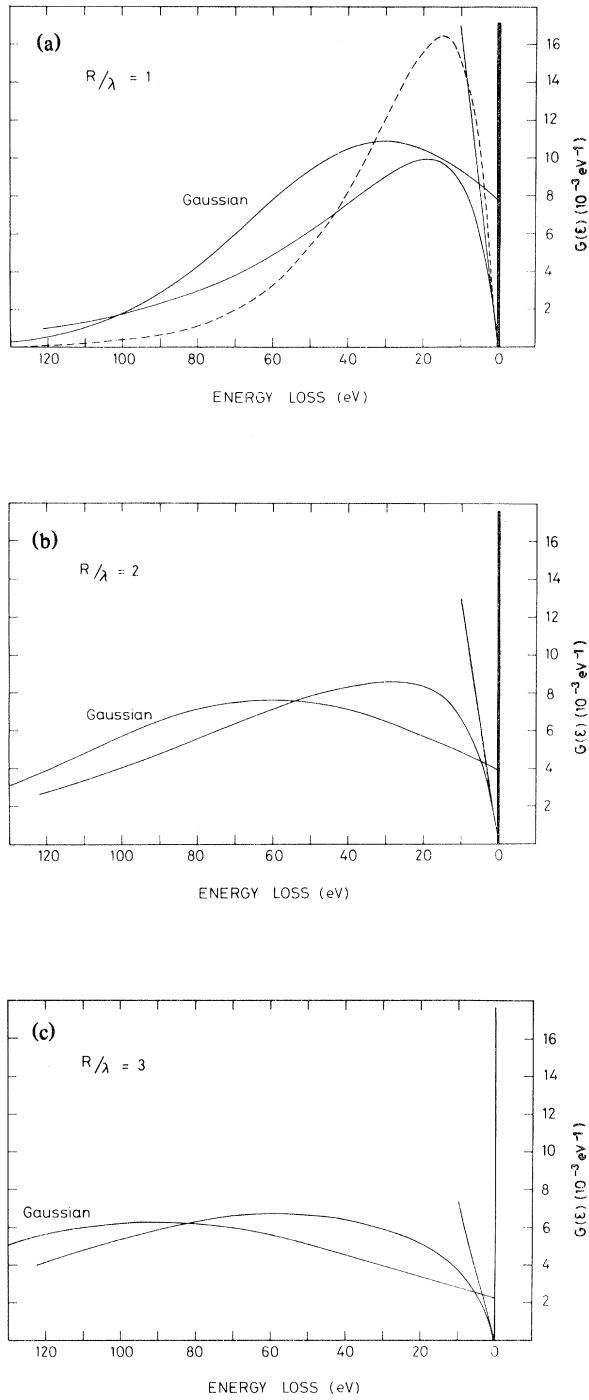


FIG. 4. (a)–(c) Energy-loss spectrum of electrons at different path lengths for the scattering model specified by Eq. (20). Full-drawn lines ending in the origin: Exact results evaluated from Eq. (24). Curves marked “Gaussian”: Evaluated from Eq. (18) with parameters according to Eq. (21). Straight lines through origin: Evaluated from linear part of Eq. (15). Dashed curve: Single-scattering spectrum, Eq. (20). Choice of $\beta^{-1} = 15 \text{ eV}$.

Insertion of (22) into (6) yields

$$G(\epsilon) = \exp\left[-\frac{AR}{\beta^2}\right] \frac{1}{2\pi} \int_{-\infty}^{\infty} ds \exp\left[is\epsilon + \frac{AR}{(\beta + is)^2}\right]. \quad (23)$$

This expression can be integrated and yields

$$G(\epsilon) = e^{-(R/\lambda)} \left[\delta(\epsilon) + \frac{2}{\lambda S} \exp\left[-\frac{2\epsilon}{\lambda S}\right] \times \sum_{\nu=1}^{\infty} \frac{(R/\lambda)^{\nu} (2\epsilon/\lambda S)^{2\nu-1}}{\nu!(2\nu-1)!} \right]. \quad (24)$$

Ignoring all energy dependence of λ , S , and W , we plot (24) in Fig. 4 for a number of values of R/λ . The respective approximated curves, (15) and (18), are also shown.

IV. ELECTRON SCATTERING

In case of an isotropic source of excited electrons, the main effect of electron scattering is to limit the contribution from deep layers to the flux of emitted electrons. This situation is quite different from the case of a collimated source where electron scattering is crucial in determining the angular distribution of emitted electrons. In view of this state of affairs, it appears justified to consider a rather simple picture of electron scattering.¹⁶

Take, for a moment, an isotropic source of electrons at depth $x=0$ in an *infinite* medium. Ignore all energy loss, but allow for angular deflection according to a differential cross section $d\sigma(\phi)$, with ϕ being the (laboratory) scattering angle. It is shown in Appendix A that the depth profile as a function of time t develops according to

$$\langle x^2 \rangle = \frac{2}{3} \nu \lambda_1 \left[t + \frac{\lambda_1}{\nu} (e^{-\nu t/\lambda_1} - 1) \right], \quad (25)$$

where

$$\frac{1}{\lambda_1} = N \int d\sigma(\phi) (1 - \cos\phi), \quad (26)$$

and $N d\sigma(\phi)$ the inverse differential mean free path for scattering ($\phi, d\phi$), i.e., N is the number of scattering centers per volume.

For small times, Eq. (25) yields

$$\langle x^2 \rangle \approx \frac{1}{3} (\nu t)^2 \quad (27)$$

corresponding to rectilinear motion, while for large t we find

$$\langle x^2 \rangle \approx 2Dt, \quad (28)$$

i.e., a diffusionlike behavior²⁰ with the diffusion coefficient

$$D = \frac{1}{3} \nu \lambda_1. \quad (29)$$

Thus, for

$$t \leq t_1 = 2\lambda_1/v, \quad (30)$$

or $R = vt \leq 2\lambda_1$, we may approximate electron trajectories as straight lines, while for $R \geq 2\lambda_1$, a diffusionlike trajectory is more appropriate.²¹

This suggests that we can approximate the depth distribution $Q(x,t)dx$ of electrons versus flight time for an isotropic source in $x=0$ by the expressions (Fig. 5)

$$Q(x,t) = \begin{cases} \frac{1}{2vt} \Theta(vt - |x|) & \text{for } t \leq t_1 \\ \frac{1}{(4\pi Dt)^{1/2}} \exp\left[-\frac{x^2}{4Dt}\right] & \text{for } t \geq t_1 \end{cases}, \quad (31)$$

so long as energy loss is neglected. Here, $\Theta(\xi)$ is the step function,

$$\Theta(\xi) = \begin{cases} 1 & \text{for } \xi > 0 \\ 0 & \text{for } \xi < 0 \end{cases}. \quad (32)$$

Consider next an isotropic source of electrons at depth $x > 0$ in a *semi-infinite* medium. Then, in the diffusion limit, we can extend (31) according to

$$Q(x',t) = \frac{1}{(4\pi Dt)^{1/2}} \left[\exp\left[-\frac{(x'-x)^2}{4Dt}\right] - \exp\left[-\frac{(x'+x)^2}{4Dt}\right] \right] \quad (33)$$

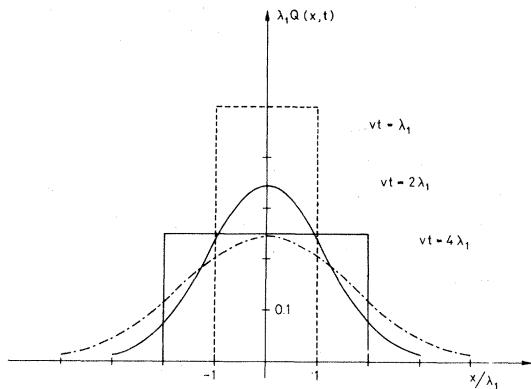


FIG. 5. Depth profiles for isotropic source of electrons in infinite medium vs flight time. Initial position $x=0$ at $t=0$, according to Eq. (31). For $vt \ll 2\lambda_1$, the profiles are approximately rectangular; for $vt \gg 2\lambda_1$, a Gaussian diffusion profile is approached. Both types of profile have been included for $vt=2\lambda_1$, indicating the magnitude of the error in the transition region. Note that all energy loss is neglected in this graph.

for $x' \geq 0$; note that we consider electrons with energies far above the work function: The surface acts as a perfectly absorbing wall.

The distribution (33) yields the following electron current through the surface at $x'=0$,

$$I(t) = -D \left. \frac{\partial Q}{\partial x'} \right|_{x'=0} = -\frac{x}{(4\pi Dt^3)^{1/2}} \exp\left[-\frac{x^2}{4Dt}\right]. \quad (34)$$

If this current has an angular distribution according to the Knudsen cosine law, we find from (34) the following probability for an electron originating at x to arrive at the surface after flight time (t,dt) under an angle $(\bar{\Omega}, d^2\Omega)$,

$$\frac{x}{(4\pi^3 Dt^3)^{1/2}} \exp\left[-\frac{x^2}{4Dt}\right] dt \cos\theta d^2\Omega. \quad (35')$$

After insertion of (29), and $dR = vdt$, we find the function Q introduced in (5) to be given by

$$Q(E_0, x; R, \bar{\Omega}) = \left(\frac{3x^2}{4\pi^3 \lambda_1 R^3} \right)^{1/2} \exp\left[-\frac{3x^2}{4\lambda_1 R}\right] \cos\theta; \quad R \geq 2\lambda_1 \quad (35)$$

in the diffusion limit for an isotropic source at x . Conversely, for straight-line motion, that function is given by

$$Q(E_0, x; R, \bar{\Omega}) = \frac{1}{4\pi} \delta(R - x/\cos\theta); \quad R \leq 2\lambda_1. \quad (36)$$

Insertion of (35) and (36) into Eq. (5), in conjunction with a properly evaluated energy spectrum (6) (see Sec. III) allows evaluation of Eq. (3).

V. HOMOGENEOUS ISOTROPIC SOURCE

Consider a homogeneous material under irradiation conditions where the attenuation length of the primary beam is much greater than the depth of emergence of electrons. For isotropic primary excitation, we can then write

$$F(E_0, \bar{\Omega}_0, x) \approx F(E_0), \quad (37)$$

so that (1) reads

$$J(E, \bar{\Omega}) = 4\pi \int dE_0 F(E_0) \int_0^\infty dx P(E_0, x; E, \bar{\Omega}). \quad (38)$$

Moreover, according to (5),

$$\int_0^\infty dx P(E_0, x; E, \bar{\Omega}) = \int_0^\infty dR G(E_0, R; E) \int_0^\infty dx Q(E_0, x; R, \bar{\Omega}) ,$$

and, according to (35) and (36),

$$\int_0^\infty dx Q(E_0, x; R, \bar{\Omega}) = \begin{cases} \frac{1}{4\pi} \cos\theta & \text{for } R \leq 2\lambda_1 , \\ \left(\frac{\lambda_1}{3\pi^3 R}\right)^{1/2} \cos\theta & \text{for } R \geq 2\lambda_1 . \end{cases} \quad (39)$$

Hence, (38) reads

$$J(E, \bar{\Omega}) = \cos\theta \int dE_0 F(E_0) \left[\int_0^{R_1} dR + \left(\frac{16\lambda_1}{3\pi}\right)^{1/2} \int_{R_1}^\infty \frac{dR}{\sqrt{R}} \right] G(E_0, R; E) . \quad (40)$$

Equation (40) has been derived in Ref. 16.

The critical path length R_1 in (40) is chosen so as to make J stationary, i.e., $\partial J/\partial R_1 = 0$, which yields

$$R_1 = \frac{16}{3\pi} \lambda_1 , \quad (41)$$

in close agreement with the previous limit $R_1 \approx 2\lambda_1$.

$$J(E, \bar{\Omega}) \approx C \cos\theta \begin{cases} \frac{1}{S} & \text{for } E_A - E < R_1 S \\ \sqrt{R_1/S} \frac{1}{(E_A - E)^{1/2}} & \text{for } E_A - E > R_1 S . \end{cases} \quad (43)$$

Equation (43) separates two regimes in the energy spectrum, a near-peak region, where the assumption of straight-line motion is adequate, and an off-peak region, where the diffusion picture is more appropriate. It is seen that the limiting energy depends on the transport mean free path λ_1 for angular deflection. For $S \sim 1 \text{ eV/\AA}$, and $\lambda_1 \geq 10 \text{ \AA}$ (for a discussion of λ_1 , see Sec. VIII), the limiting energy loss is $\geq 20 \text{ eV}$. Therefore, within the range of validity of these estimates, it appears justified to ignore angular deflection in the analysis of measured spectra in the immediate vicinity of a peak, *if the target is homogeneous*.

B. Near-peak regime

Consider now the spectrum in the immediate vicinity of the peak at E_A . Inserting (15) into (40), and setting $R_1 \approx \infty$ we find

$$J(E, \bar{\Omega}) \approx C \cos\theta \lambda \{ \delta(E_A - E) + A \lambda (E_A - E) \times [+ \frac{1}{6} A^2 \lambda^2 (E_A - E)^3] \cdots \} , \quad (44)$$

A. Straight-path versus diffusion regime

Consider first the continuous-slowning-down distribution Eq. (18') and a delta-function source,

$$F(E_0) = C \delta(E_0 - E_A) , \quad (42)$$

with some constant C . Then, (18'), (40), and (42) yield

indicating that a background signal $\sim A \lambda (E_A - E)$ is superimposed on the primary peak signal. Concerning terms of higher order, see Sec. VD below.

C. Off-peak regime

Consider now the opposite limit of energy losses exceeding both the limit defined by Eq. (43) and that of (12), i.e., the continuum portion of the observed spectrum. Insertion of (18) into (40), and setting $R_1 \approx 0$ yields

$$J(E, \bar{\Omega}) \approx C \cos\theta \left(\frac{32\lambda_1}{3\pi^2 W}\right)^{1/2} e^{\epsilon S/W} K_0(\epsilon S/W) , \quad (45)$$

where K_0 is a modified Bessel function of the third kind, and

$$\epsilon = E_A - E . \quad (45a)$$

For $\epsilon \gg W/S$, the asymptotic expansion of K_0 is

valid, so that

$$J(E, \vec{\Omega}) \approx C \cos\theta \left(\frac{16\lambda_1}{3\pi S} \right)^{1/2} \frac{1}{(E_A - E)^{1/2}}, \quad (45b)$$

i.e., the lower part of Eq. (43), while for $\epsilon \leq W/S$ we find

$$J(E, \vec{\Omega}) \approx C \cos\theta \left(\frac{32\lambda_1}{3\pi^2 W} \right)^{1/2} \ln \frac{W}{S(E_A - E)}. \quad (45c)$$

Thus, the continuum portion of the spectrum not too far away from the peak varies logarithmically with the inverse energy loss.

$$J(E, \vec{\Omega}) \approx 4C \cos\theta \left(\frac{\lambda\lambda_1}{3} \right)^{1/2} \left[\delta(\epsilon) + \frac{2}{\lambda S} \exp\left(-\frac{2\epsilon}{\lambda S}\right) \sum_1^\infty \frac{(\epsilon/\lambda S)^{2\nu-1}}{\nu!(\nu-1)!} \right] \quad (46b')$$

in the diffusion limit. Obviously, (46a) applies to small, and (46b') to large values of ϵ , i.e., the delta function term in (46b') needs to be ignored. Thus, (46b') takes on the final form

$$J(E, \vec{\Omega}) \approx 4C \left(\frac{\lambda\lambda_1}{3} \right)^{1/2} \cos\theta \frac{2}{\lambda S} \exp\left(-\frac{2\epsilon}{\lambda S}\right) I_1\left(\frac{2\epsilon}{\lambda S}\right), \quad (46b)$$

where I_1 is a modified Bessel function of the first kind. Expansion of (46a) for small ϵ reveals that the linear term in ϵ agrees with that in (44) while the square term does not occur in (44). This demonstrates that (44), which originates from an expansion

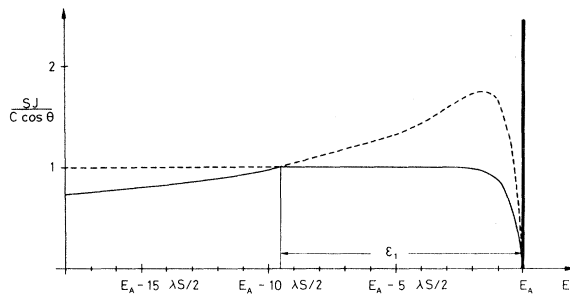


FIG. 6. Calculated energy spectrum of electrons emitted from a solid containing an homogeneous isotropic source of electrons at a primary energy E_A . Evaluated from Eqs. (46a) and (46b), based on inelastic scattering model, Eq. (20). The abscissa scale can be compared with that in Fig. 4 by setting $\lambda S/2 = 15$ eV. The two approximate curves, Eqs. (46a) and (46b), have been fully drawn in their respective regimes of validity ($E \gtrsim \epsilon_1$), and stippled otherwise. For $\lambda_1/\lambda = 3$.

D. Analytical example

While analytical evaluation of Eq. (40) for the spectrum (24) is possible in principle, the result is not particularly enlightening except for the limits $R_1 = \infty$ and $R_1 = 0$, respectively. Here, one finds

$$J(E, \vec{\Omega}) \approx C \lambda \cos\theta \left\{ \delta(\epsilon) + \frac{1}{\lambda S} \left[1 - \exp\left(-\frac{4\epsilon}{\lambda S}\right) \right] \right\} \quad (46a)$$

for straight-line motion and

for small R , Eq. (15), is not a proper power series in ϵ . This is the reason for the square brackets in Eq. (44).

Figure 6 shows the two spectra, (46a) and (46b), for the special case of $\lambda_1 = 3\lambda$. Equation (41) predicts the near-peak regime to extend down to $E = E_A - \epsilon_1$ with $\epsilon_1 \approx 16\lambda S/\pi$. This is seen to be the case. Also, the transition between the two regimes is rather smooth. Figure 7 shows the transition point ϵ_1 that separates the near-peak regime from the off-peak regime as a function of the ratio λ_1/λ , for $\lambda_1/\lambda > 1$.

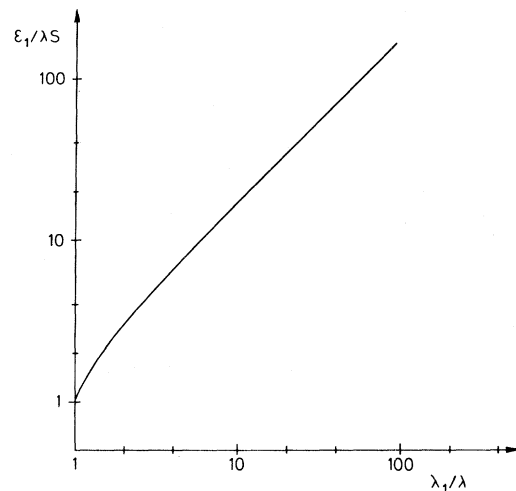


FIG. 7. Critical energy loss ϵ_1 separating near-peak from off-peak regime, corresponding to negligible influence of angular deflection and diffusion model of angular deflection, respectively, as a function of ratio of transport and inelastic mean free path, λ_1/λ . Evaluated for inelastic scattering model, Eq. (20).

VI. INHOMOGENEOUS SOURCE: PEAK ATTENUATION

Consider an inhomogeneous isotropic source, e.g., a sample with a nonuniform depth profile of the emitting species. Then, the electron spectrum is, in general, given by

$$J(E, \vec{\Omega}) = 4\pi \int dE_0 \int dx F(E_0, x) \int dR Q(E_0, x; R, \vec{\Omega}) G(E_0, R; E) , \quad (47)$$

according to Eqs. (1), (2), and (5).

If only the zero-loss peak is considered, Eq. (15) yields

$$\int_{E \approx E_A} G(E_A, R; E) dE = e^{-R/\Lambda} , \quad (48)$$

and hence,

$$\int_{E \approx E_A} J(E, \vec{\Omega}) dE = 4\pi \int_0^\infty dx F(x) \int dR e^{-R/\Lambda} Q(E_A, x; R, \vec{\Omega}) , \quad (49)$$

for a monochromatic source. Evaluation of the integral over dR (49) by means of (35) and (36) yields (cf. Appendix B)

$$\int_0^\infty dR e^{-R/\Lambda} Q(E_A, x; R, \vec{\Omega}) \approx \begin{cases} \frac{1}{4\pi} \exp\left(-\frac{x}{\lambda \cos\theta}\right) & \text{for } x \ll R_1 \\ \frac{1}{\pi} \cos\theta \exp\left(-\frac{x}{(\lambda\lambda_1/3)^{1/2}}\right) & \text{for } x \gg R_1 \end{cases} \quad (50)$$

under the assumption that $\lambda_1 > \lambda$. After integration over $d^2\Omega$, (49) and (50) yield

$$\int d^2\Omega \int_{E \approx E_A} dE J(E, \vec{\Omega}) \approx 4\pi \left[\int_0^{x_1} dx F(x) \frac{1}{2} E_2\left(\frac{x}{\lambda}\right) + \int_{x_1}^\infty dx F(x) \exp\left(-\frac{x}{(\lambda\lambda_1/3)^{1/2}}\right) \right] , \quad (51)$$

where x_1 is defined by the relation

$$\frac{1}{2} E_2\left(\frac{x_1}{\lambda}\right) = \exp\left(-\frac{x_1}{(\lambda\lambda_1/3)^{1/2}}\right) , \quad (51a)$$

and

$$E_2(\xi) = \int_1^\infty dt e^{-t\xi/t^2} .$$

It is seen that the attenuation of the zero-loss signal is determined by the inelastic mean free path λ for shallow layers ($x \ll x_1 \approx R_1$), but by the characteristic depth Λ with

$$\Lambda = (\lambda\lambda_1/3)^{1/2} , \quad (52)$$

at greater depths ($x \gg x_1$). As a rough approximation, one may approximate (51) by

$$\int d^2\Omega \int_{E \approx E_A} dE J(E, \vec{\Omega}) \approx 4\pi \int_0^\infty dx \frac{F(x)}{1 + e^{x/\Lambda}} , \quad (51')$$

where the weight function shows the right limiting value at $x=0$ and the correct asymptotic behavior for $x \gg x_1$.

As an example, consider a dilute alloy, doped with a steplike concentration profile of some dopant so

that

$$F(x) = \begin{cases} 0 & \text{for } x < X \\ C & \text{for } x > X \end{cases} , \quad (52')$$

if the observed Auger or XPS line originates from the dopant. In this case, the parameter Λ is a matrix

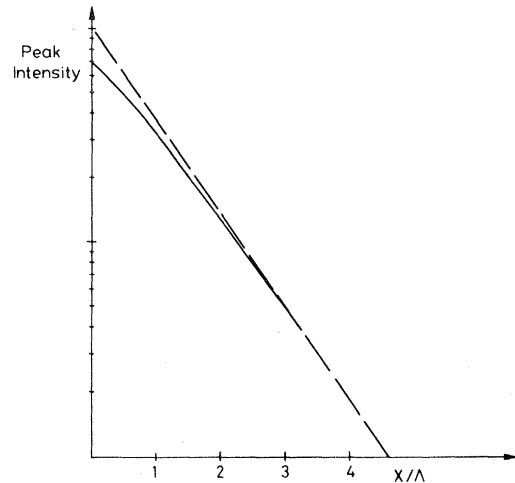


FIG. 8. Intensity of the zero-loss peak as a function of overlayer thickness X , according to Eq. (53). Escape depth Λ according to Eq. (52). The dashed curve is an exponential, $\text{const exp}(-X/\Lambda)$.

property. Integration of (51') on the basis of (52') yields

$$\int d^2\Omega \int_{E=E_A} dE J(E, \vec{\Omega}) \approx 4\pi C \Lambda \ln(1 + e^{-X/\Lambda}) \quad (53)$$

Thus, the peak intensity decreases with increasing thickness X of the dopant-free overlayer. This decrease is exponential for $X \gg \Lambda$ but less pronounced for $X \leq \Lambda$ (Fig. 8).

VII. LINE-SHAPE ANALYSIS

We return to an homogeneous medium and consider a primary excitation spectrum $F(E_0)$ with a narrow but nonzero width and some built-in structure. In the vicinity of the peak, we may disregard angular deflection of the emitted electrons, i.e., set $R_1 = \infty$ in Eq. (40). Hence, according to (12), the spectrum (40) can be written in the form

$$J(E, \vec{\Omega}) \approx \lambda \cos\theta \int dE_0 F(E_0) \left[\delta(E_0 - E) + \lambda K(E_0 - E) + \lambda^2 \int dT K(T) K(E_0 - E - T) \dots \right] \quad (54)$$

Usually, only relative current measurements will be performed. Hence, introducing the quantity

$$j(E) = \frac{J(E, \vec{\Omega})}{\lambda \cos\theta} \quad (55)$$

we can write (54) in the form

$$j(E) \approx F(E) + \lambda \int dE_0 F(E_0) \left[K(E_0 - E) + \lambda \int dT K(T) K(E_0 - E - T) \dots \right] \quad (56)$$

As an example, take a Gaussian primary spectrum

$$F(E) = \frac{1}{\sqrt{2\pi}\Delta E} \exp\left[-\frac{(E - E_1)^2}{2\Delta E^2}\right] \quad (57)$$

and a loss function according to Eq. (20).

Thus, Eqs. (40) and (24) yield the following spectrum in the near-peak region,

$$\begin{aligned} j(E) &= F(E) + \frac{1}{\lambda S} \int_E^\infty dE_0 F(E_0) \left[1 - \exp\left[-\frac{4(E_0 - E)}{\lambda S}\right] \right] \\ &= F(E) + \frac{1}{2\lambda S} \left[\operatorname{erfc}\left(\frac{E - E_1}{\sqrt{2}\Delta E}\right) - \exp\left(\frac{4(E - E_1)}{\lambda S} + \frac{8\Delta E^2}{\lambda^2 S^2}\right) \operatorname{erfc}\left(\frac{E - E_1 + 4\Delta E^2/\lambda S}{\sqrt{2}\Delta E}\right) \right] \quad (58) \end{aligned}$$

where

$$\operatorname{erfc}(x) = \frac{2}{\sqrt{\pi}} \int_x^\infty dt e^{-t^2} \quad (59)$$

This situation is illustrated in Fig. 9 for two values of the ratio $\Delta E/\lambda S$. Figure 9(a) shows a rather broad initial spectrum, where the measured electron spectrum contains a significant background. In Fig. 9(b), where $\Delta E/\lambda S = 0.25$, a well-pronounced peak is ob-

served, superimposed on an approximately linear background.

Figure 9 shows also a number of simplified approximations to the spectrum. First, the single-scattering spectrum, following by truncating the series (56),

$$j(E) \approx F(E) + \int_E^\infty dE_0 F(E_0) \lambda K(E_0 - E) \quad (60)$$

reads

$$j(E) \approx F(E) \left[1 + \left(\frac{2\Delta E}{\lambda S}\right)^2 \right] - \frac{1}{2} \left(\frac{2}{\lambda S}\right)^2 \left[E - E_1 + \frac{2}{\lambda S} \Delta E^2 \right] \exp\left[\frac{2(E - E_1)}{\lambda S} + \frac{1}{2} \left(\frac{2\Delta E}{\lambda S}\right)^2\right] \operatorname{erfc}\left(\frac{E - E_1 + 2\Delta E^2/\lambda S}{\sqrt{2}\Delta E}\right) \quad (60a)$$

after insertion of the primary spectrum (57) and the loss function (20). It is seen that (60a) describes the peak shape rather well, in particular in the case of the narrower peak, Fig. 9(b).

The linear approximation (14) to the loss function yields

$$j(E) \approx F(E) \left[1 + \left(\frac{2\Delta E}{\lambda S}\right)^2 \right] - \frac{1}{2} \left(\frac{2}{\lambda S}\right)^2 (E - E_1) \operatorname{erfc}\left(\frac{E - E_1}{\sqrt{2}\Delta E}\right) \quad (60b)$$

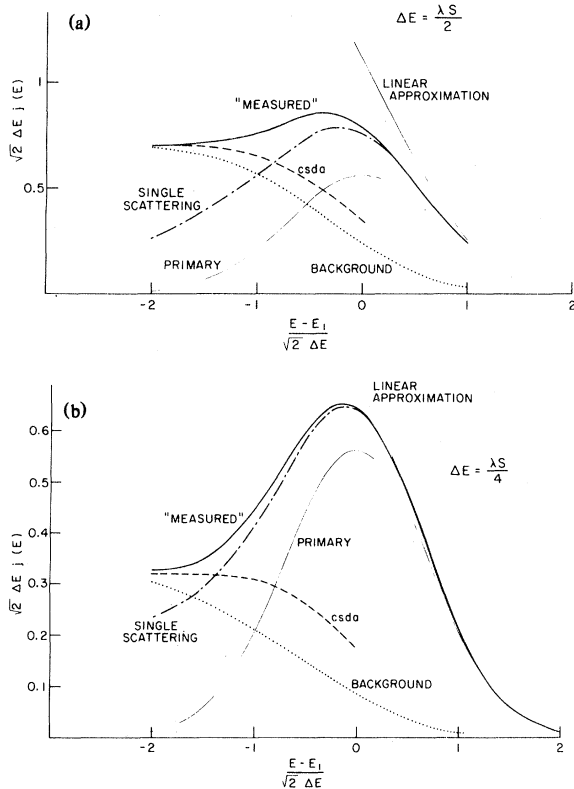


FIG. 9. Calculated electron spectrum in the near-peak region for Gaussian primary spectrum, Eq. (57). For a loss function (20), the "measured" spectrum is given by Eq. (58). The difference between that spectrum and the primary one, i.e., the correction term in Eq. (58), is labeled "background." Curves labeled "single scattering" refer to Eqs. (60) and (60a), while the linear approximation reflects Eq. (60b). Curves labeled "csda" (continuous-slowing-down approximation) are based on Eqs. (61) and (61a). ΔE is the width of the primary spectrum (57), and λS the mean energy loss per inelastic scattering event. (a) $\Delta E = \lambda S/2$; (b) $\Delta E = \lambda S/4$.

instead of (60a), under otherwise identical assumptions. It is seen that this approximation only describes the high-energy side of the peak. It will have to be discarded for most applications.

Finally, we have also included a curve based upon the continuous-slowing-down approximation (18') where

$$j(E) \approx \frac{1}{\lambda S} \int_E^\infty dE_0 F(E_0), \quad (61)$$

i.e.,

$$j(E) \approx \frac{1}{4} \frac{2}{\lambda S} \operatorname{erfc} \left(\frac{E - E_1}{\sqrt{2} \Delta E} \right) \quad (61a)$$

in the case of the primary spectrum (57). This spectrum is, by the very nature of its origin, more appropriate to characterize the background signal at

large energy losses rather than the complete spectrum, and it is obvious that it defines accurately the asymptotic value of $j(E)$ below the peak.

The same expression, Eq. (61), follows if (18') is replaced by (18).

As a reasonable first-order approximation, we can adopt (60) and (61) above and below the crossing point of the two spectra, respectively.

The fact that (60) describes the central parts of the peak rather well, especially for narrow peaks, suggests that the inverse relation to Eq. (56), can also be truncated at lowest order, i.e.,

$$F(E) \approx j(E) - \int_E^\infty dE_0 j(E_0) \lambda K(E_0 - E). \quad (62)$$

This relation allows, in principle, deduction of the primary spectrum $F(E)$ from a measured electron current $j(E)$.

The main attractive feature of Eq. (62) is the fact that only the relative loss function $\lambda K(E_0 - E)$, rather than the absolute one, occurs. Indeed, in view of (11), we have

$$\int_0^\infty dT \lambda K(T) = 1. \quad (63)$$

Thus, if only the *shape* of the energy-loss spectrum is known within the range of energy losses that contribute substantially to the total inverse mean free path, Eq. (62) allows an inversion of $j(E)$ into $F(E)$.

Finally, we demonstrate that unlike (60), which is a first-order approximation, Eq. (62) is actually *rigorous* within the near-peak region, i.e., so long as angular deflections can be ignored. Starting from Eq. (40) for $R_1 = \infty$, we have

$$j(E) = \frac{1}{\lambda} \int dE_0 F(E_0) \int_0^\infty dR G(E_0, R; E); \quad (64)$$

Eq. (6) yields

$$\int_0^\infty dR G(E_0, R; E) = \frac{1}{2\pi} \int_{-\infty}^\infty ds e^{is(E_0 - E)} \frac{1}{\Sigma(s)}. \quad (65)$$

Insertion of (65) into (64), and Fourier transform with respect to E yields

$$\lambda \Sigma(s) \int dE e^{isE} j(E) = \int dE_0 F(E_0) e^{isE_0}. \quad (66)$$

Fourier transform with respect to s yields, then,

$$F(E) = \frac{1}{2\pi} \int_{-\infty}^\infty ds e^{-isE} \lambda \Sigma(s) \int dE' e^{isE'} j(E'). \quad (67)$$

After insertion of Eq. (8), the integral over s can be performed, and the result is

$$F(E) = j(E) - \int_E^\infty dE' j(E') \lambda K(E' - E), \quad (68)$$

which is identical with (62), except that we now deal with a much more rigorous relationship.

Equation (68) has formally a similar appearance to

Shirley's inversion formula¹⁰ which, in the present notation, reads

$$F(E) = j(E) - \int_E^\infty dE' j(E') \kappa, \quad (69)$$

where κ is a constant,

$$\kappa = j(E_2) \left(\int_{E_2}^\infty dE' j(E') \right)^{-1}, \quad (69a)$$

and E_2 the lower energy limit at which the primary spectrum $F(E)$ has dropped to zero. We may conclude that Eq. (69) represents an accurate procedure for background subtraction *only* in case of a loss function that is uniform in *energy loss* over an interval comparable to the width of the primary spectrum.

VIII. DISCUSSION

It may be appropriate at this point to comment on the various mean free paths entering our treatment, i.e., primarily the inelastic mean free path λ , the transport mean free path λ_1 , and the escape depth, $\Lambda = (\lambda\lambda_1/3)^{1/2}$ [cf. Eq. (52)].

Calculations have been performed²²⁻²⁵ of the *inelastic mean free path* λ , mainly on the basis of the dielectric theory of the electron gas,²⁶ but in some cases with the inclusion of atomic core excitations. The dependence of λ on electron energy turns out to show a characteristic minimum at an electron energy around 50 eV, which is also observed for experimental values of the *escape depth* Λ .²⁷ Nevertheless, the identification of the measured escape depth with the inelastic mean free path²² is conceptually an oversimplification, as follows from Eq. (52). To what extent there exists a quantitative similarity depends on the behavior of the transport mean free path, λ_1 .

The transport mean free path is determined by the frequency of angular deflections and is thus dependent on both inelastic and elastic scattering events. Although the importance of the latter has been well established in connection with the slowing down of β particles,^{19,20} it has not always been fully appreciated in the field of electron emission and electron spectroscopy.²⁸ Calculations for a random scattering medium²⁴ indicate that the mean free path for elastic collisions, λ_e , for Al is smaller than λ at all energies; the difference is particularly pronounced at energies below the minimum in λ . Similar conclusions emerge from calculations on crystalline media.²⁹

In addition to some uncertainty about the mechanism of elastic or quasielastic (phonon) scattering in a solid at electron energies in the range of 50–1500 eV, there is also a difference between λ_e and λ_1 due to the cosine term in Eq. (26). Figure 10 shows the ratio λ_1/λ_e calculated for exponentially screened Coulomb interaction with a screening radius a , based on Born approximation.³⁰ It is seen that the difference is negligible at low energies, but is substantial

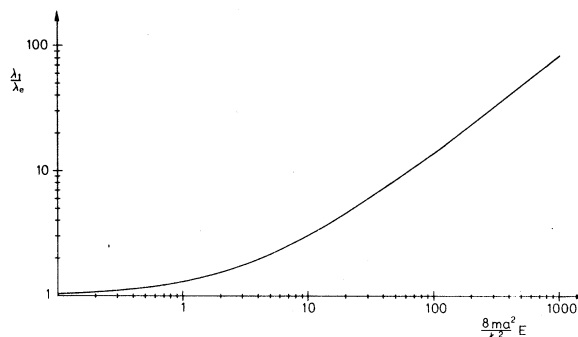


FIG. 10. Ratio between transport mean free path λ_1 for angular deflection, Eq. (26), and mean free path for angular deflection, $\lambda_e = [N \int d\sigma(\phi)]^{-1}$, calculated for elastic scattering on screened Coulomb potential, $V(r) = \text{const} \times r^{-1} \exp(-r/a)$ by first Born approximation.

for

$$E > \frac{\hbar^2}{8ma^2} \approx \frac{Z^{2/3}}{4} \mathcal{R}, \quad (70)$$

where Z is the atomic number and $\mathcal{R} = 13.6$ eV. This, in fact, makes λ_1 approach the inelastic mean free path λ at energies *above* the minimum of λ . Still, the behavior at energies below the minimum of λ is very different.²⁴ This, as well as the numerical factor $1/\sqrt{3}$ in Eq. (52), suggests that the apparently good agreement between measured escape depths and calculated mean free paths²² may be fortuitous.

At this point, we should like to put emphasis on the fact that our energy-loss function (20) was chosen for analytical convenience in order to test the validity of various approximations. Although the qualitative features of this function reflect the general behavior of simple systems, the quantitative features definitely do not. The peak shape expressed by Eq. (20) may well be much too broad in comparison with the predictions of Refs. 18 and 22; conversely, the dropoff at higher energies is too rapid in comparison with the T^{-2} dependence expected for Coulomb scattering. Moreover, all complex structure has been smeared out in Eq. (20). Thus, while we find this spectrum very well suited for qualitative considerations such as those expressed by Figs. 4, 6, 7, and 9, we wish to express strong reservations with regard to the prospects of extracting, e.g., primary spectra from measured currents on the basis of Eq. (20) with A and β determined by "experimental" values of λ and S .

We note that a considerable amount of information on slowing-down parameters is contained in the off-peak region as well as the region far below the peak.^{16,31} In particular, we believe that proper analysis of electron spectra is one of the few possibilities to determine λ_1 for electron scattering in solids experimentally in the energy range under consideration. We intend to follow up on the problem of extracting *both* the primary spectrum *and* the slowing-

down parameters in a consistent manner from measured electron spectra in subsequent work.

IX. SUMMARY

(i) We have analyzed theoretically the spectrum of electrons emitted from solids in the case where the primary spectrum is narrow, such as is the case in x-ray photoelectron and Auger electron spectroscopy.

(ii) We distinguish between the near-peak region, the off-peak region, and the region far below the peak. The near-peak region is dominated by electrons emitted from shallow layers that may have lost energy but have not undergone substantial angular deflection.

The off-peak region is dominated by electrons that have undergone angular deflection but have lost only a small fraction of their initial energy.

The region far below the peak is made up by electrons coming from deeper layers that have lost a substantial fraction of their energy. At the lowest energies secondary electrons also contribute to this group.

(iii) Unlike in our previous work,¹⁶ we considered only the near-peak and the off-peak region. Therefore, all variations of slowing-down parameters, i.e., inverse differential mean free path $K(T)$, inelastic mean free path λ , stopping power S , straggling parameter W , differential scattering cross section $d\sigma(\phi)$, and transport mean free path λ_1 , with the *energy of the moving electrons* was ignored. This is an essential condition for validity both of the Landau formula of energy loss, Eq. (6), and the evaluation of the scattering distribution, Eq. (25).

(iv) For a homogeneous and isotropic source strength, the electron spectrum is given by Eq. (40) where R_1 is the critical traveled path length separating the regimes of negligible and non-negligible angular deflection, respectively. $G(E_0, R; E) dE$ is the probability for an electron with initial energy E_0 to have an energy (E, dE) after traveling a path length R .

(v) The critical energy loss ϵ_1 separating the near-peak from the off-peak region is of the order of $\epsilon_1 \approx 2\lambda_1 S$ [cf. Eq. (41) and Fig. 7 which has been calculated on the basis of a specific model for the energy loss].

(vi) The function $G(E_0, R; E)$ is discussed in Sec. III. We distinguish between a low-energy-loss region where G is dominated by structural features in the cross section $K(T)$ [see Eq. (12)], and a higher-energy-loss region where a continuum description of energy loss is appropriate, see Eqs. (18) and (18').

(vii) Energy spectra in the near-peak region have been investigated in some detail (Secs. VB, VD, and VII), both as a function of traveled path length (Fig. 4), and as a function of emitted energy; the latter spectrum is shown for a primary excitation of zero width (Fig. 6) as well as two examples of Gaussian excitation profiles [Figs. 9(a) and 9(b)]; in both

cases, the half-width at half maximum is smaller than the mean energy loss per inelastic scattering, λS . All calculations refer to a specific model for the loss function.

(viii) Energy spectra in the off-peak region have been discussed less extensively, see Fig. 6 and Eqs. (45)–(45c). This region has been treated on the basis of the familiar diffusion approximation for the scatter distribution of electrons. The main feature is a decreasing contribution of deeper layers to the spectrum at any given energy and, therefore, a decrease in the spectral density with increasing energy loss. A logarithmic variation, Eq. (45c), is predicted in the region next to the near-peak region.

(ix) A formula has been derived, Eq. (68), that allows direct inversion of a measured electron spectrum into an (unknown) primary excitation function, provided that the normalized loss function $\lambda K(T) dT$ is known, T being the energy loss in an inelastic scattering event. The inversion formula is rigorous within the near-peak region.

(x) With a view to the physical significance of published values of the escape depth of Auger and photoelectrons, we also evaluated the intensity of the zero-loss peak as a function of the thickness of a passive overlayer on an homogeneous target. The overlayer was assumed to have the same slowing-down parameters as the matrix. We find the attenuation to be dominated by the inelastic mean free path λ only within a very shallow range of thicknesses, while the major portion of the attenuation function is found to be exponential with a decay length $\Lambda = (\lambda\lambda_1/3)^{1/2}$ [cf. Eq. (52)], where λ_1 is the transport mean free path for elastic scattering.

(xi) Figure 9 shows that the attenuation function deviates from a strict exponential in a thickness range of the order of λ .

(xii) A qualitative discussion of mean free paths based on existing theoretical literature suggests that it is not in general justified to identify the escape depth measured by means of overlayers with the inelastic mean free path.

ACKNOWLEDGMENTS

Our thanks are due to our colleagues H. F. Winters and P. Morgen for drawing to our attention some unsolved problems in electron spectroscopy, to R. H. Ritchie for numerous pieces of advice, and to I. Alstrup, I. Chorkendorff, A. Ignatiev, J. Onsgaard, C. J. Powell, W. N. Unertl, and K. B. Winterbon for valuable comments on this work.

APPENDIX A: DERIVATION OF EQ. (25)

We consider the motion of an electron in an homogeneous, infinite medium. The motion is character-

ized by a distribution function $G(\vec{v}_0, \vec{v}, \vec{r}, t) d^3v d^3r$ of the velocity and position vectors \vec{v} and \vec{r} at time t , \vec{v}_0 is the initial velocity at $t=0$ where the electron is assumed to be at $\vec{r}=0$.

The function G obeys Boltzmann's equation which we use in the backward form,³²

$$\left[-\frac{1}{v_0} \frac{\partial}{\partial t} - \frac{\vec{v}_0}{v_0} \cdot \vec{\nabla} \right] G(\vec{v}_0, \vec{v}, \vec{r}, t) = N \int d\sigma (G(\vec{v}_0, \vec{v}, \vec{r}, t) - G(\vec{v}', \vec{v}, \vec{r}, t)) , \quad (\text{A1})$$

where \vec{v}' is the velocity after a scattering event characterized by a cross section $d\sigma(\vec{v}, \vec{v}')$. Furthermore,

$$G(\vec{v}_0, \vec{v}, \vec{r}, 0) = \delta(\vec{v} - \vec{v}_0) \delta(\vec{r}) . \quad (\text{A2})$$

For planar geometry we integrate over all directions of \vec{v} to obtain an equation with the energy E as a variable. Further if we assume that the cross section for *angular deflection* depends only weakly on electron energy within an interval of, say, $0.75E_0 \leq E \leq E_0$, we may integrate over E and write

$$\left[-\frac{\partial}{\partial R} - \eta_0 \frac{\partial}{\partial x} \right] G(\eta_0, x, R) = N \int d\sigma (G - G') \quad (\text{A3})$$

and

$$G(\eta_0, x, 0) = \delta(x) , \quad (\text{A4})$$

where η_0 and η' are directional cosines with respect to the x axis, G' stands for G with $\eta_0 = \eta'$, R is the travelled path length, and $d\sigma$ is now the cross section for angular deflection.

Now, expand G in terms of Legendre polynomials and take spatial moments, i.e.,

$$G(\eta_0, x, R) = \sum_{l=0}^{\infty} (2l+1) G_l(x, R) P_l(\eta_0) \quad (\text{A5})$$

$$P(x, \vec{\Omega}) = \frac{1}{4\pi} \int_0^{R_1} e^{-R/\lambda} \delta(R-x/\eta) + \left[\frac{3x^2\eta^2}{4\pi^3\lambda_1} \right]^{1/2} \int_{R_1}^{\infty} dR e^{-R/\lambda} R^{-3/2} \exp\left[-\frac{3x^2}{4\lambda_1 R} \right] , \quad (\text{B1})$$

where $\eta = \cos\theta$ and R_1 is given by (41). For the second integral we have

$$B(x) \leq \left[\frac{3x^2\eta^2}{4\pi^3\lambda_1} \right]^{1/2} \int_{R_1}^{\infty} dR e^{-R/\lambda} R^{-3/2} = \left[\frac{3x^2\eta^2\lambda^2}{4\pi^3\lambda_1 R^3} \right]^{1/2} \exp\left[-\frac{R_1}{\lambda} \right] , \quad \text{for } R_1 > \lambda . \quad (\text{B2})$$

and

$$G_l^n(R) = \int dx x^n (G_l(x, R)) . \quad (\text{A6})$$

Then, Eqs. (A5) and (A4) readily read³³

$$-(2l+1) \frac{\partial G_l^n}{\partial R} + n l G_l^{n-1} + n(l+1) G_l^{n+1} = (2l+1) N \sigma_l G_l^n \quad (\text{A7})$$

and

$$G_l^n(0) = \delta_{n0} \delta_{l0} , \quad (\text{A8})$$

where

$$\sigma_l = \int d\sigma [1 - P_l(\cos\phi)] , \quad (\text{A9})$$

and ϕ is the scattering angle in the laboratory frame.

For $n=0$, Eqs. (A7) and (A8) yield

$$G_l^0(R) = \delta_{l0} ,$$

i.e., conservation of particle number. For $l=n=1$ and $l=0, n=2$, we obtain the differential equations

$$\frac{\partial G_1^1}{\partial R} + N \sigma_1 G_1^1 = \frac{1}{3} \quad (\text{A10})$$

and

$$\frac{\partial G_0^2}{\partial R} = 2G_1^1 , \quad (\text{A11})$$

respectively, which are readily solved.

For an isotropic source

$$\langle x^2 \rangle^2 = G_0^2 = \frac{2}{3N\sigma_1} \left[R - \frac{1}{N\sigma_1} (1 - e^{-N\sigma_1 R}) \right] , \quad (\text{A12})$$

where the right-hand expression results from (A10) and (A11) with the initial condition (A8).

APPENDIX B: RANGE OF VALIDITY OF EQ. (50)

The propagator function is according to Eqs. (35) and (36) given by

Then, for $x \ll R_1$ we find

$$P(x, \vec{\Omega}) = \frac{1}{4\pi} \int_0^{R_1} e^{-R/\lambda} \delta(R-x/\eta) = \frac{1}{4\pi} \exp\left[-\frac{x}{\lambda\eta} \right] , \quad (\text{B3})$$

since according to (B2),

$$B(x) \ll \exp\left[-\frac{x}{\lambda\eta} \right] \quad \text{for } x \ll R_1 .$$

For $x \gg R_1$, the first integral is zero, and because the maximum in the second integrand occurs for $R \gg R_1$ we may extend the lower bound of this integral to zero. Thus,

$$P(x, \vec{\Omega}) \approx \left(\frac{3x^2 \eta^2}{4\pi^3 \lambda_1} \right)^{1/2} \int_0^\infty dR e^{-R/\lambda} R^{-3/2} \exp\left(-\frac{3x^2}{4\lambda_1 R}\right) = \frac{\eta}{\pi} \exp\left(-\frac{x}{(\lambda\lambda_1/3)^{1/2}}\right). \quad (\text{B4})$$

- ¹L. Fiermanns, J. Vennik, and W. DeKeyser *Electron and Ion Spectroscopy of Solids* (Plenum, New York, 1978).
- ²L. A. Harris, *J. Appl. Phys.* **39**, 1419 (1968); T. W. Haas and J. T. Grant, *Appl. Phys. Lett.* **16**, 172 (1970).
- ³R. E. Weber and A. L. Johnson, *J. Appl. Phys.* **40**, 314 (1969).
- ⁴J. T. Grant, T. W. Haas, and J. E. Houston, *Phys. Lett.* **45A**, 309 (1973).
- ⁵G. D. Mahan, *Phys. Rev.* **163**, 612 (1967); P. Nozières and C. T. de Dominicis, *ibid.* **178**, 1097 (1969); S. Doniach and M. Sunjic, *J. Phys. C* **3**, 285 (1970).
- ⁶G. K. Wertheim and S. Hüfner, *Phys. Rev. Lett.* **35**, 53 (1975).
- ⁷P. H. Citrin, G. K. Wertheim, and Y. Baer, *Phys. Rev. B* **16**, 4256 (1977).
- ⁸P. Staib and J. Kirschner, *Appl. Phys.* **3**, 421 (1974).
- ⁹E. N. Sickafus, *Surf. Sci.* **100**, 529 (1980).
- ¹⁰D. A. Shirley, *Phys. Rev. B* **5**, 4709 (1972).
- ¹¹E. N. Sickafus, *Phys. Rev. B* **16**, 1436 (1977).
- ¹²C. N. Berglund and W. E. Spicer, *Phys. Rev.* **136**, A1030 (1964).
- ¹³H. H. Madden and J. E. Houston, *J. Appl. Phys.* **47**, 307 (1976).
- ¹⁴R. P. Vasquez, J. D. Klein, J. J. Barton, and F. J. Grunthaner, *J. Electron Spectrosc. Relat. Phenom.* **23**, 63 (1981).
- ¹⁵J. A. D. Matthew and P. R. Underhill, *J. Electron Spectrosc. Relat. Phenom.* **14**, 371 (1978).
- ¹⁶P. Sigmund and S. Tougaard, in *Inelastic Particle-Surface Collisions*, Chemical Physics Series, Vol. 17, edited by E. Taglauer *et al.* (Springer, Berlin, 1981), p. 2.
- ¹⁷L. Landau, *J. Phys. (Moscow)* **8**, 201 (1944).
- ¹⁸C. J. Tung and R. H. Ritchie, *Phys. Rev. B* **16**, 4302 (1977).
- ¹⁹N. Bohr, *K. Dan. Vidensk. Selsk. Mat.-Fys. Medd.* **18**, No. 8 (1948).
- ²⁰H. A. Bethe, M. E. Rose, and L. P. Smith, *Proc. Am. Philos. Soc.* **78**, 573 (1938).
- ²¹In Ref. 20, it is shown that, in the limit of long times, Boltzmann's equation approaches the diffusion equation. In order to set an estimate of the time required we extended the procedure described in Appendix A to the fourth moment, $\langle x^4 \rangle$, and obtained
- $$\langle x^4 \rangle \sim \frac{1}{3} \left(\frac{2R}{N\sigma_1} \right)^2 + \frac{16(\sigma_1 - 5\sigma_2)R}{15(N\sigma_1)^3\sigma_2}$$
- for large R . The term $\propto R^2$ is readily shown to yield the correct kurtosis of a (Gaussian) diffusion profile. Thus, a necessary condition for (33) to be accurate is
- $$R \gg \frac{1}{N\sigma_1} \left| \frac{4}{5} \frac{\sigma_1}{\sigma_2} - 4 \right|.$$
- This requirement is somewhat more stringent than $R > R_1$, with R_1 given by Eq. (41). In practice, deviations appear to be small (cf. Fig. 7).
- ²²R. H. Ritchie, C. J. Tung, V. E. Anderson, and J. C. Ashley, *Radiat. Res.* **64**, 181 (1975); J. C. Ashley, C. J. Tung, and R. H. Ritchie, *Surf. Sci.* **81**, 409, 427 (1979).
- ²³D. R. Penn, *Phys. Rev. B* **13**, 5248 (1976).
- ²⁴J. P. Ganachaud and M. Cailler, *Surf. Sci.* **83**, 498 (1979); M. Cailler, J. P. Ganachaud, and J. P. Bourdin, *Thin Solid Films* **75**, 181 (1981).
- ²⁵D. L. Lin and D. F. Stickland, *J. Appl. Phys.* **51**, 1286 (1980).
- ²⁶J. Lindhard, *K. Dan. Vidensk. Selsk. Mat.-Fys. Medd.* **28**, No. 8 (1954).
- ²⁷P. W. Palmberg and T. N. Rhodin, *J. Appl. Phys.* **39**, 2425 (1968); Y. Baer, P. F. Heden, J. Hedman, M. Klasson, and C. Nordling, *Solid State Commun.* **8**, 1479 (1970); M. L. Tarng and G. K. Wehner, *J. Appl. Phys.* **44**, 1534 (1973); F. L. Battye, J. S. Jenkin, J. Liesegang, and R. C. G. Leckey, *Phys. Rev. B* **9**, 2887 (1974); C. J. Powell, *Surf. Sci.* **44**, 29 (1974); M. P. Seah and W. A. Dench, *Surf. Interface Anal.* **1**, 2 (1979); K. Nishimori, H. Tokutaka, and K. Takashima, *Surf. Sci.* **100**, 665 (1980); C. D. Wagner, L. E. Davis, and W. M. Riggs, *Surf. Interface Anal.* **2**, 53 (1980).
- ²⁸Some attention was given to the effect of elastic scattering on electron spectra in Ref. 12, although the postulated factorization of the effects of elastic and inelastic scattering in the measured spectra is not confirmed by the present work where factorization is claimed only at any given path length, see Eq. (15). With regard to *angular-resolved* photoelectron spectroscopy, considerable attention was given to elastic scattering by N. J. Shevchik [*Phys. Rev. B* **16**, 3428 (1977)] and N. J. Shevchik and D. Liebowitz [*Phys. Rev. B* **18**, 1618, 1630 (1978)]. See also O. A. Baschenko and V. I. Nefedov, *J. Electron Spectrosc. Relat. Phenom.* **17**, 405 (1979).
- ²⁹M. B. Webb and M. G. Lagally, in *Solid State Physics: Advances in Research and Applications*, Vol. 28 edited by H. Ehrenreich *et al.* (Academic, New York, 1973), p. 301.
- ³⁰L. I. Schiff, *Quantum Mechanics* (McGraw-Hill, New York, 1949).
- ³¹J. Schou, *Phys. Rev. B* **22**, 2141 (1980).
- ³²E.g., P. Sigmund, *Rev. Roum. Phys.* **17**, 823 (1972).
- ³³E.g., K. B. Winterbon, P. Sigmund, and J. B. Sanders, *K. Dan. Vidensk. Selsk. Mat.-Fys. Medd.* **37**, No. 14 (1970).